Biochimica et Biophysica Acta 1804 (2010) 362–373

Contents lists available at ScienceDirect

Biochimica et Biophysica Acta

journal homepage: www.elsevier.com/locate/bbapap

Review

Structure and catalytic mechanism of the β-carbonic anhydrases

Roger S. Rowlett *

Colgate University, Department of Chemistry, 13 Oak Drive, Hamilton, NY 13346, USA

ARTICLE INFO

Article history:
Received 23 June 2009
Received in revised 30 July 2009
Accepted 2 August 2009
Available online 11 August 2009

Keywords:
β-Carbonic anhydrase
Carbon dioxide
Bicarbonate
Catalytic mechanism
Kinetics
Allostery

ABSTRACT

The β-carbonic anhydrases (β-CAs) are a diverse but structurally related group of zinc-metalloenzymes found in eubacteria, plant chloroplasts, red and green algae, and in the Archaea. The enzyme catalyzes the rapid interconversion of CO_2 and H_2O to HCO_3^- and H^+, and is believed to be associated with metabolic enzymes that consume or produce CO_2 or HCO_3^-. For many organisms, β-CA is essential for growth at atmospheric concentrations of CO_2. Of the five evolutionarily distinct classes of carbonic anhydrase, β-CA is the only one known to exhibit allosterism. Here we review the structure and catalytic mechanism of β-CA, including the structural basis for allosteric regulation.

1. Introduction

The first β-carbonic anhydrase (CA) was unwittingly discovered by Neish in 1939 [1] as a constituent of plant leaf chloroplasts. Remarkably, plant chloroplastic CA would not be recognized as an evolutionarily and structurally distinct form of carbonic anhydrase until some 5 decades later, with the advent of DNA sequencing technology. At that time, it was the second evolutionarily distinct form of CA known, hence the β-designation. Since 1990, many demonstrated and putative β-CAs have been discovered not only in photosynthetic organisms, but also in eubacteria, yeast, and archaeal species. Perhaps like no other class of CA, the β-enzyme exhibits a broad structural and functional diversity. There have been other excellent reviews of the possible physiological function and relationship of β-CA to other classes of CA [2–6], so this review will focus primarily on the structure and catalytic mechanism of this unique CA.

2. Brief history and significance

2.1. Discovery and distribution

The existence of CA in plants–one variant of the enzyme that would be later recognized as a β-CA–was first established in 1939 [1]. In 1990, the cDNA sequence for spinach (*Spinacea oleracea*) chloroplast CA was determined, and found to be non-homologous to animal (α) CA [7]. Shortly thereafter, highly homologous cDNA sequences of pea (*Pisium sativum*) [8,9] and *Arabidopsis thaliana* CAs [10,11] were reported. While these enzymes would be the three plant β-CAs to be most well-characterized, many others have been identified genomically, and are variously believed to be distributed in the chloroplastic stroma, thylakoid space, and cytoplasm [12].

The first bacterial CA to be recognized as a β-CA was the *CynT* gene of *Escherichia coli* [13]. More than a dozen eubacterial β-CAs are now known [14,15], including enzymes from common pathogens such as *Helicobacter pylori*, *Mycobacterium tuberculosis*, and *Salmonella typhimurium*. β-CAs are also known in the Archaea (*Methanobacterium thermoautotrophicum*) [16], in yeast (*Saccharomyces cerevisiae*) [17], cyanobacteria (*Synechocystis* PCC6803) [18], carboxysomes of chemoautotrophic bacteria (*Halothiobacillus neapolitanus*) [19], and in green (*Chlamydomonas reinhardtii*) [20] and red (*Porphyridium purpureum*) [21] algae.

2.2. Early structural insights

The plant CAs were the first β-CAs to be structurally characterized. Plant β-CA was recognized as a zinc-metalloenzyme as long ago as

Abbreviations: CA, carbonic anhydrase; EXAFS, extended X-ray absorption fine structure; Rubisco, ribulose-1,5-bisphoshate carboxylase; HICA, *Haemophilus influenzae* β-CA; ECCA, *Escherichia coli* β-CA; MTCA, *Methanobacterium thermoautotrophicum* β-CA; PPCA, *Porphyridium purpureum* β-CA; PSCA, *Pisium sativum* β-CA; HTCA, *Halothiobacillus neapoliatanus* β-CA; Rv3588, *Mycobacterium tuberculosis* Rv3588 β-CA; Rv1284, *Mycobacterium tuberculosis* Rv1284 β-CA; HCAII, human α-CA II; ATCA, *Arabidopsis thaliana* β-CA; SOCA, *Spinacea oleracea* β-CA; HEPES, 4-(2-hydroxyethyl)piperazineethanesulfonic acid; MOPS, 2-(*N*-morpholino)ethanesulfonic acid

* Corresponding author. Tel.: +1 315 228 7245; fax: +1 315 228 7935.
E-mail address: rrowlett@colgate.edu.

1570-9639/$ – see front matter © 2009 Elsevier B.V. All rights reserved.
doi:10.1016/j.bbapap.2009.08.002

1946 [22]. More quantitative measurements of zinc, conducted more than two decades later [23–25], suggested that there was one zinc ion per protein subunit. Bacterial β-CAs have likewise been demonstrated to be zinc-metalloenzymes. Unlike γ- and δ-CAs–enzymes that have been shown to tolerate zinc in the active site, but *in vivo* appear to utilize iron [26] and cadmium[27], respectively–all metal-characterized β-CAs appear to be zinc-metalloenzymes.

When cDNA nucleotide sequences of plant β-CAs became available, it seemed unlikely from the deduced amino acid sequence that the zinc ligands in β-CA would be the canonical $His_3(H_2O)$ coordination sphere found in α-CAs [28]. EXAFS studies of spinach β-CA [29,30] show clear differences from that of human α-CA I [31]: the first shell peak of the radial distribution curve is significantly broader in spinach β-CA than in human α-CA I, and is best modeled by an equal number of metal ion ligands at 2.3 and 2.0 Å, respectively; the second shell EXAFS peak, where the backscatter from the β-carbons of His ligands are prominent, is much weaker for spinach β-CA than for human α-CA I. The first shell scattering distances are consistent with a four-coordinate geometry which includes Zn–S and Zn–(O/N) ligands, and the most likely coordination sphere–assuming there must be a catalytically essential water molecule present–is $Cys_2His(H_2O)$. This coordination sphere was thought to be unique among CAs–α-, γ- [32] and δ-CAs [33] are all known to have $His_3(H_2O)$ coordination spheres–until the structural characterization of ζ-CA, a cadmium metalloenzyme that has the same coordination sphere as β-CA [27].

2.3. Significance of β-CA

Demonstrating the precise physiological role(s) of β-CA has remained somewhat elusive, although it is likely to be an important accessory enzyme for many CO_2 or HCO_3^- utilizing enzymes, *e.g.*, Rubisco in chloroplasts, cyanase in *E. coli* [34], urease in *H. pylori* [35], and bicarbonate-dependent carboxylases in *Corynebacterium glutamicum* [36]. β-CA is an essential component of the carboxysome, a CO_2 concentrating organelle in cyanobacteria; mutation of this β-CA produces a phenotype that requires high concentrations of CO_2 for growth [37]. It has also been demonstrated that β-CA is essential for growth in *E. coli* [38], *C. glutamicum* [36], and *S. cerevisiae* [39] under aerobic conditions and atmospheric concentrations of CO_2. In β-CA deficient mutants of *S. cerevisiae*, it has been shown that wild-type or catalytically competent variants of α- or β-CA can restore the ability of the organism to grow under aerobic conditions [40]. *H. pylori* has not one but two CAs, a periplasmic α-CA and an intracellular β-CA; inhibition of these enzymes with sulfonamides inhibits growth *in vitro* [35].

In higher plants, the importance of β-CA is not as yet clearly demonstrated. Antisense constructs of tobacco (*Nicotiana tabacum*) expressing as little as 1% of the normal chloroplast β-CA levels had no demonstrable effect on carbon assimilation [41]. However, it has been shown that Rubisco and β-CA are transcriptionally linked in *P. sativum*: when plants are transferred from an environment with high CO_2 to one with atmospheric (low) CO_2, both Rubisco and β-CA expression levels increase together [42].

3. Structure

Astonishingly, it took a full decade after the recognition of the existence of β-CA as a structurally independent form of the enzyme to obtain an X-ray crystal structure of a representative of this CA class. This was in no small part due to the circumstance that the plant enzymes were the β-CAs upon which most of the initial research focused; unfortunately, the plant β-CAs are somewhat difficult to handle, and are quite sensitive to air oxidation. To date, there is still only one plant β-CA that has been successfully characterized by X-ray diffraction.

The first reported β-CA X-ray structure was that of *P. purpureum*, a red alga, in 2000 [21]. This was quickly followed by structures for a plant (*P. sativum*) [43] and a bacterial (*E. coli*) [44] β-CA. As of this writing, 6 additional β-CA X-ray crystal structures are known, including in order of appearance, an archaeal β-CA (*M. thermoautotrophicum*) [45], two enzymes from *M. tuberculosis* [46], one of which is observed to crystallize in two different active site and oligomerization structures [47], a carboxysomal β-CA (*H. neapolitanus*) [19], and *Haemophilus influenzae* β-CA [48].

3.1. The fundamental structural unit of β-CA is a dimer

All β-CAs share a unique α/β fold not found in any other proteins. Although β-CA can adopt a variety of oligomeric states with molecular masses ranging from 45 to 200 kDa, the fundamental structural unit appears to be a dimer or its structural equivalent. In the case of PSCA, ECCA, HICA, Rv1284, Rv3588, and MTCA, the fundamental dimer is composed of two identical protein chains; in the case of PPCA and HTCA, the fundamental structural unit is a pseudo-dimer in which a monomer has apparently been gene-duplicated and then concatenated to form a pseudo-dimer with approximately 2-fold symmetry. The pseudo-monomers can be highly homologous–the tandem repeat in PPCA has ≈70% sequence identity between the N- and C-terminal portions of the pseudo-dimer [49]–or can exhibit significant divergence—HTCA has only 11% identity between its pseudo-monomeric units [19]. Fig. 1 shows ribbon diagrams of the fundamental dimers of β-CAs whose structures have been determined by X-ray diffraction.

All β-CAs share a common structural element composed of a central parallel β-sheet composed of four strands in a 2-1-3-4 arrangement within each monomer or pseudo-monomer. In some β-CAs, a fifth, anti-parallel β-strand (β5) associates with β4. With the exception of HTCA, the parallel β-sheets in each monomer or pseudo-monomer are arranged in a roughly anti-parallel fashion to form an extended, 8–10 strand β-sheet core that extends across the fundamental structural unit. Numerous α-helices pack onto this β-sheet core; these helices and strand β5 comprise the surface of the fundamental dimer or pseudo-dimer. The fundamental dimer or pseudo-dimer is tightly entwined: there are extensive monomer–monomer contacts in the region where the parallel β-sheets adjoin; in addition, two N-terminal α-helices wrap around and clasp the neighboring monomer, where α1 interacts with β4 and β5. The surface area [50] of this "dimerization" interface is approximately 3000 $Å^2$ in HICA, ECCA, 1EKJ, and MTCA. In Rv3588, the dimerization contact area is smaller, just over 1600 $Å^2$, while in Rv1284 it is much larger, over 3700 $Å^2$.

Nearly all the structurally characterized β-CAs contain one zinc ion per monomer or pseudo-monomer that is in a pseudo-tetrahedral coordination environment of the type $Cys_2His(X)$, where X is water, an anion, or an Asp residue. This zinc ion defines the location of the active site of the enzyme. The lone exception is HTCA, in which the pseudo-2-fold symmetry between the pseudo-monomeric units has been broken. HTCA is a unique member of the β-CA class. Indeed, it is so unique that it was originally thought to be an evolutionarily distinct form of the enzyme designated ε-CA [51]. However, the X-ray structure reveals that HTCA is a β-CA in which one of the pseudo-monomers has evolutionarily diverged to the point that it has lost all of its zinc ligands, including an entire loop that normally harbors the last Cys ligand [19]. HTCA is composed of three domains: an unusual N-terminal 4-helix bundle with α-helices of greatly varying lengths; a middle, catalytic domain that is structurally homologous to other β-CAs, and includes a catalytic zinc ion; and a C-terminal domain that is weakly homologous to the catalytic domain and contains the classic 2-1-3-4 β-CA β-sheet, but does not have a properly constituted active site or zinc coordination sphere.

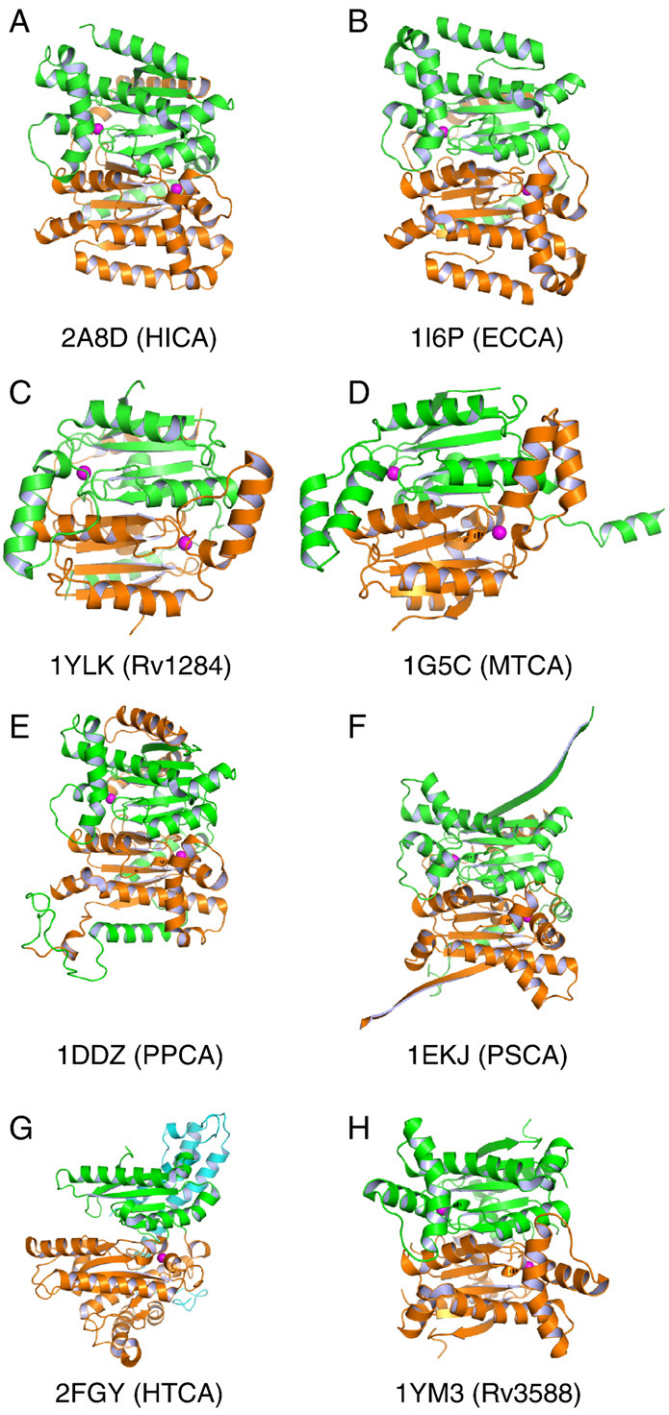

Fig. 1. Ribbon diagrams of the fundamental dimers of structurally characterized β-CAs. Structures are labeled by their PDB accession codes with origin in parentheses. HICA, chains D (green) and F (orange); ECCA, chain A (green) and its symmetry partner (orange); Rv1284, chains A (green) and B (orange); MTCA, chains A (green) and B (orange); PPCA, chain A, N-terminal domain (84–316, orange) and C-terminal domain (317–564, green); PSCA, chains G (green) and H (orange); HTCA, chain A, N-terminal domain (38–144, cyan), catalytic domain (151–397, orange), C-terminal domain (398–514, green); Rv3588, chain A (green) and its symmetry partner (orange). Zinc ions are shown as magenta spheres.

3.2. Oligomerization of β-CAs

Among the structurally characterized β-CAs are enzymes whose biological units appear to be dimers, tetramers and octamers. The oligomerization state appears to be driven by surface extensions or unique elaborations of the secondary structure of the basic β-CA fold, as described in the following sections. Fig. 2 shows van der Waals surface depictions of the most common oligomeric forms of β-CA.

3.2.1. Tetramers

The most common arrangement for β-CA is a tetramer (HICA, ECCA, Rv1284) or a pseudo-tetramer composed of two pseudo-dimers (PPCA, HTCA). The "tetramerization" interface is orthogonal to the dimerization interface, and is composed of α-helical segments that form a relatively flat face on the fundamental dimer. The surface area [50] of this contact interface is ≈1600–1700 Å^2 for HICA, ECCA and Rv1284, or ≈800–850 Å^2 per monomer, about one-third to one-quarter of the area of the dimerization interface. The PPCA tetramerization interface has a larger surface are of ≈4700 Å^2, or ≈2350 Å^2 per pseudo-monomer. It thus seems likely that the forces maintaining tetramers are somewhat weaker than those maintaining dimer formation. HTCA also forms a pseudo-tetramer by association of its two pseudo-dimers through an interface with a surface area [50] of 1450 Å^2, or 725 Å per pseudo-monomer. The loss of tetramerization contact area compared to homotetrameric β-CAs is accounted for by the deletion of a significant part of the structure of the C-terminal pseudo-monomeric domain of HTCA.

3.2.2. Octamers

The biological unit of PSCA is an octamer with 222 symmetry [43]. A structural feature of PSCA, one that appears to be uniquely shared with dicotyledenous but not monocotyledonous plant chloroplastic enzymes, is an extended C-terminus that forms a long β5 strand. An anti-parallel β5–β5′ interaction is responsible for the association of dimers into higher-order structures. Two different types of β5–β5′ interactions are required to assemble the PCSA octamer. The first of these involves a "tetramerization" interface along a crystallographic 2-fold axis in which there is a significant amount of interaction area [50] (≈1700 Å^2) between the two dimers, including the β5–β5′ interaction. The second involves an "octamerization" interface which is primarily mediated by a slightly different β5–β5′ interaction. The total contact area between dimers on this interface is ≈1300 Å^2 [50]. The resulting octamer is remarkably intertwined: each PSCA monomer in the complex makes contacts with 5 adjoining monomers [43].

3.2.3. Dimers

Two structurally characterized β-CAs can exist in dimeric forms. MTCA forms crystals with one homodimer per asymmetric unit [45]. This enzyme has significantly truncated N- and C-termini compared to other β-CAs. As a result it is missing the equivalent of α1 and α2 segments that assist in dimerization by clasping the neighboring monomer. This role is taken up instead by residues 90–125, which form two helices, α4 and α5, that partially extend over the neighboring monomer on the expected tetramerization interface. The position of these helices would appear to preclude tetramerization of the enzyme in a manner similar to HICA, ECCA, or PPCA. MTCA is also missing the extended β5 segment that is essential for octamer formation in PSCA. In the crystal structure, the N-terminal helix of chain A is domain-swapped with its nearest neighbor in the crystal. The N-terminal helix of chain B packs against β4 and β5, analogous to tetrameric and octameric β-CAs; in aqueous solution, it seems likely that the N-terminal helix of chain A of MTCA is arranged similarly to that of chain B. Although gel exclusion chromatrography [16] and ultracentrifugation [52] suggest that MTCA may exist in solution as a tetramer, the crystal structure suggests that a tetrameric form like that of HICA, ECCA, PPCA, or Rv1284 is unlikely because of the disruption of the tetramerization interface by α4 and α5.

Native Rv3588 crystallizes a monomer [46] that can clearly form a dimer but not a tetramer with symmetry partners in the unit cell. Surprisingly, the thiocyanate complex of the same enzyme crystallizes as a dimer of dimers [47] in the asymmetric unit with classic 222 symmetry. The tetramerization interface of Rv3588 is stabilized by a large network of salt bridges in which positively charged residues (mostly Arg) outnumber negatively charged residues (Asp and Glu) 20

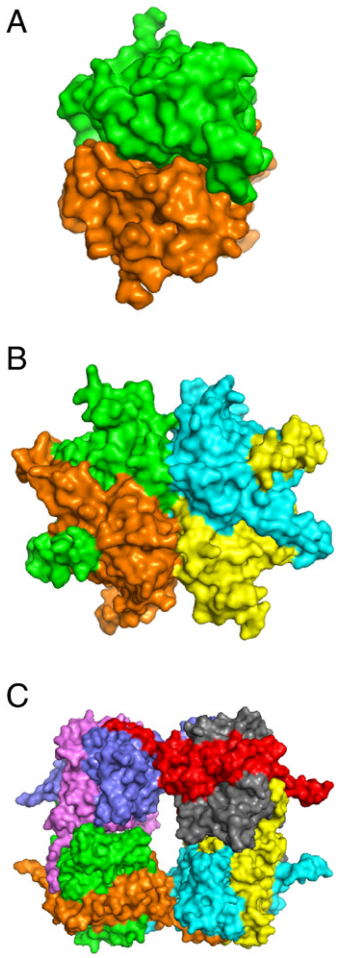

Fig. 2. Oligomeric forms of β-CA. (A) Rv3588 dimer. Dimerization interface is horizontal; tetramerization interface is right-hand face. (B) HICA tetramer. One fundamental dimer is green and orange, the other is yellow and cyan. Dimerization interfaces are horizontal; tetramerization interface is vertical. (C) PSCA octamer. Fundamental dimers are orange/green, light blue/pink, red/gray, and yellow/cyan. The tetramerization interfaces are along the horizontal crystallographic 2-fold axis; the octamerization interfaces are along the vertical non-crystallographic 2-fold axis.

to 12. Dynamic light scattering studies [47] show that the tetrameric form of the enzyme dissociates into dimers as the pH is lowered from pH 8.4 to 7.5, and that this quaternary structure change is associated with changes in zinc ligation sphere. It is possible that Rv3588 requires high pH for tetramerization in order to maximize the neutralization of excess positive charge in the tetramerization interface [47].

3.3. Post-translational modification of β-CA in plants

The chloroplastic β-CAs from higher plants are encoded in the nucleus and synthesized as precursor molecules that contain a serine/threonine-rich chloroplastic transit peptide [7,8,10,53,54]. β-CAs isolated from *S. oleracea* and *P. sativum* indicate that the proteolytic processing of these chloroplastic peptides may be heterogeneous; native PSCA in particular can be isolated in two distinct molecular weight forms [54], and it appears that the proteolysis of the transit peptide may occur in two separate steps [55]. The heterogeneity of native PSCA does not appear to affect the oligomerization or catalytic activity of the enzyme [54].

3.4. There are two structural classes of β-CA

The extant X-ray crystal structures of β-CA appear to fall into two distinct structural classes as determined by the organization of the active site region in its uncomplexed state, designated here as "type I" and "type II" β-CA. The principal differences between these two types of β-CA relate to the ligation state of the active site zinc ion, and the orientation and organization of nearby residues. Each structural class of β-CA will be described based on an archetypical representative, with selected parallels drawn for other representatives of the same class. Table 1 lists structurally equivalent amino acid residues in each of the 8 structurally characterized β-CAs, as well as one additional kinetically characterized β-CA to help clarify discussion.

3.4.1. Type I β-CAs

3.4.1.1. PSCA. Type I β-CA is typified by PSCA; other CAs in this structural class include MTCA, Rv1284, and HTCA. Fig. 3A depicts the active site structure of PSCA. In PSCA, the active site zinc ion is located on the fundamental dimer interface, and is ligated to Cys160, His220, and Cys223; a fourth coordination site can be occupied by acetic acid,

Table 1
Functionally equivalent residues in selected structurally or kinetically characterized β-CAs.

	Type I β-CAs					Type II β-CAs		
	PSCA	ATCA	MTCA	Rv1284	HTCA	HICA & ECCA	PPCA	Rv3588
Zn ligands	C160	C167	C32	C35	C173	C42	C149/403	C51
	D162[a]	D169[a]	D34[a]	D37[a]	D175[a]	D44	D151/405	D53
	H220	H227	H87	H88	H242	H98	H205/459	H104
	C223	C230	C90	C91	C253	C101	C208/462	C107
Active site	Q151′	Q158′	H23′	P25′	H397	Q33′	Q394/140	Q32′
	D162	D169	D34	D37	D175	D44	D151/405	D53
	S163	S170	S35	A38	G177	S45	S152/406	S54
	R164	R171	R36	R39	R177	R46	R153/407	R55
	G224	G231	G91	G92	A254	G102	G209/463	G108
Active site cleft	F179′	F186′	K53′	H54′	Y418	F61′	F422/168	F70′
	V184	I191	A58	A59	A200	V66	I173/427	A75
	Y205′	Y212′	V72′	I73′	V434	Y83′	Y444/190	Y89′
	H209′	H216′	S76	L77	I438	V87′	Y448/194	V93′
Non-catalytic HCO_3^- binding pocket[b]	V157	V164	I32	I32	I170	W39	W146/400	I56
	A159	A166	T31	A34	P172	G41	G148/402	G58
	V165	V172	L38	L40	L176	V47	V154/408	V64
	R182	R189	K56	R57	A198	R64	R171/425	R81
	Y307	Y314	I156	F151	V295	Y181	Y289/543	Y187

Numbers with primes indicate residues from a neighboring monomer in the fundamental dimer.
[a] This residue does not act as a zinc ligand in this enzyme; it is included here for comparison purposes only.
[b] Only HICA and ECCA have been demonstrated to have a non-catalytic HCO_3^- binding pocket; residues from other enzymes are shown for comparison purposes only.

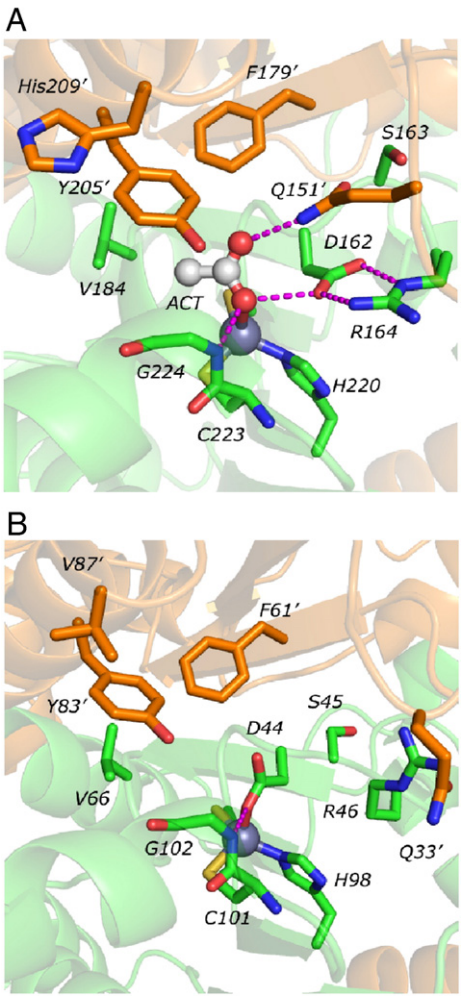

Fig. 3. Active site structures of representative types I and II β-CA. (A) PSCA (PDB 1EKJ), chains G and H, ACT is acetate; (B) HICA (PDB 2A8D), chains D and F. The active site monomer is colored green; the neighboring monomer is colored orange. Residues in the neighboring monomer are numbered with primes. Magenta dashes indicate hydrogen bonding interactions.

or acetate ion–a bicarbonate analog–which is present in the crystallization solution. A constellation of polar side chains and main-chain atoms stabilizes the binding of acetic acid to the zinc ion. In chain G of PSCA, one oxygen of Asp162 is positioned to accept a hydrogen bond from the zinc-bound –OH of acetic acid. Asp162 is oriented in this position by Arg164 with which it forms two hydrogen bonds to the guanidinium group. The same –OH oxygen of acetic acid also accepts a hydrogen bond from the main-chain amide of Gly224. Finally, the side-chain amide of Gln151′ donates a hydrogen bond to the other oxygen of acetic acid. The active site cleft leading from bulk solution to the zinc ion leads along the dimerization interface and is quite constricted; it is lined with hydrophobic residues, including Phe179′, Val184, and Tyr205′. The only polar residue in the cleft is His209′, which lies near the exterior of the active site opening. The bottom of the cleft, near the zinc ion, is too narrow to accommodate CO_2 or HCO_3^-: presumably the side chains lining this cleft must rearrange to accommodate the binding of substrate and release of product. Remarkably, the active site of PSCA functionally maps rather accurately onto the active site of human α-CA II (HCAII) [43], an enzyme for which the mechanism of action is well-understood. The most significant of these mappings are Oδ1 of Asp162 in PSCA onto Oγ1 of Thr199 in HCAII, and the side-chain amide of Gln151′ in PSCA onto the main-chain amide of Thr199 in HCAII. In HCAII, the Oγ1 of Thr199 donates a hydrogen bond to Glu106, and is therefore an obligate hydrogen bond acceptor for the oxygen atom bound to the zinc ion; it has been proposed to act as a "gatekeeper" residue by excluding from the zinc ligand environment anions that cannot donate a hydrogen bond at this position. Clearly, the Oδ1 of Asp162 in PSCA could perform a similar role in PSCA. The main-chain amide of Thr199 is observed to donate a hydrogen bond to zinc-bound bisulfate in HCAII, and has been proposed to be important in stabilizing the transition state leading from CO_2 to bicarbonate during catalysis; in PSCA, the side-chain amide of Gln151′ plays a similar role, providing a hydrogen bond to the O atom of the zinc-bound acetic acid. Notably, both Asp162 and Gln151 are highly conserved in β-CAs. MTCA, Rv1284, and HTCA all follow the archetype of PSCA, with a few significant differences.

3.4.1.2. MTCA. In MTCA, Cys32, His87, and Cys90, and a water molecule are the zinc ligands, and Arg36 orients Asp34 to interact with the zinc-bound water. His23′ is the equivalent for Gln151′ in PSCA, but has been oriented away from the active site by the domain swapping of the N-terminal helix in the crystal structure. Instead, the sulfonate group of an enzyme-bound HEPES molecule in MTCA occupies the equivalent position of Gln151′ in PSCA. The active site cleft of MTCA is still constricted, but significantly roomier than that of PSCA, due to the substitutions of Lys53′ for Phe179′, Ala58 for Val184, and Val72′ for Tyr205′ in MTCA for PCSA, respectively.

3.4.1.3. Rv1284. The Rv1284 enzyme is closely related to MTCA. It also has a zinc-ligand environment that coordinates a water molecule as the fourth ligand, joining Cys35, His90, and His93. Asp34 and Arg36 form a dyad which allows Asp34 to interact with the zinc-bound water. Unlike all other β-CAs, Rv1284 does not have a residue at a position analogous to Gln151′ in PSCA to donate a hydrogen bond to a zinc-bound bicarbonate ion: the analogous residue in Rv1284 is Pro26. However, like MTCA, the active site cleft in Rv1284 is more open than in PSCA, with His54′, Ala83, and Ile73′ substituting for the bulkier Phe179′, Val184, and Tyr205′ in PSCA.

3.4.1.4. HTCA. Carboxysomal HTCA has less than 15% sequence identity with other β-CAs, and has numerous insertions and deletions in the typical β-CA sequence, including the loss of a catalytic site in its C-terminal domain. Nevertheless, HTCA maintains an active site structure in its catalytic domain that is surprisingly structurally homologous with other type I β-CAs. The catalytic zinc ion is coordinated by Cys173, His242, and Cys253; unlike other β-CAs, there is a long intervening sequence between the last two metal ligands. The fourth metal coordination site is occupied by a water molecule, which is pinned by hydrogen bonds donated by the amide of Ala254 and accepted by Asp175. Like other type I β-CAs, this Asp residue forms a dyad with Arg177, which helps orient it for an interaction with the zinc-bound water. Like MTCA, His397 is positioned where Gln151′ is located in PSCA, where it could donate a hydrogen bond to zinc-bound bicarbonate ion. Finally, the constricted active site cleft along the pseudo-dimer interface of the catalytic and C-terminal domains is lined by hydrophobic residues, including Ala200, Tyr418, Val434, and Ile438. Tellingly, the corresponding "cleft" residues for the defunct, catalytically incompetent C-terminal domain have significantly diverged to Tyr195, His421, Ala211, and Lys215. These residues, rather than forming narrow hydrophobic cleft leading to a second active site, now occupy the surface of a very large cavity on the pseudo-dimer interface opposite the single active site.

3.4.1.5. Summary of type I β-CA structure. Type I β-CAs are characterized by the following active site features: (1) a four-coordinate $Cys_2His(X)$ coordination sphere where X is an exchangeable ligand (*e.g.*, acetate, acetic acid, water); and (2) an Asp-Arg dyad that serves to orient the Asp residue to accept a hydrogen bond from the exchangeable ligand atom bound directly to the zinc ion; (3) a hydrogen bond donor

positioned to interact with a zinc-bound bicarbonate ion in the exchangeable ligand position, and (4) a narrow, hydrophobic active site cleft that lies along the dimer or pseudo-dimer interface, and leads to the active site zinc ion.

3.4.2. Type II β-CAs

3.4.2.1. HICA and ECCA. Type II β-CAs are typified by HICA and ECCA, which have nearly identical sequences and structures, and do not require separate discussion. Other members of this structural class include PPCA and Rv3588. Fig. 3B depicts the active site structure of HICA. As for type I β-CAs, the active site in HICA is located on the dimerization interface, and contains a zinc ion. In contrast to type I β-CAs, the active site zinc ion in HICA is coordinated to 4 protein ligands: Cys42, Asp44, His98, and Cys101. There are no other zinc ligands. The zinc-bound Asp residue is the same residue that forms the Asp-Arg dyad in type I β-CAs. In HICA, this dyad interaction is broken, and Arg46, the other half of the erstwhile dyad, is rotated away. In addition, Gln33′–analogous to Gln151′ in PSCA–is also rotated away from the active site region. In PSCA, Ser163 donates a hydrogen bond to the side-chain carbonyl of Gln151′, orienting it appropriately to donate a hydrogen bond to a zinc-bound acetic acid (or bicarbonate ion). In HICA, the 44–48 loop has been rotated by about 90° such that Ser45–the HICA analog for Ser162 in PSCA–is no longer in a position to interact with Gln33′. However, the hydrogen bond between the main-chain amide of Gly102 and the zinc-bound oxygen atom of Asp44 is retained, and is analogous to the interaction of Gly224 with the zinc-bound oxygen atom of acetic acid in PSCA. HICA also retains the narrow, hydrophobic active site cleft of type I β-CAs, including residues Phe61′, Val66, Tyr83′, and Val87′. In HICA, the channel leading to the active site is exceedingly narrowed at the bottom, too small even for a water molecule to pass through in the crystal structure; therefore it must be assumed that the bulky, hydrophobic residues must slightly rearrange to accommodate substrate for catalysis.

3.4.2.2. PPCA. The active site organization of PPCA is directly analogous to that of HICA. The zinc ion has a closed pseudo-tetrahedral coordination shell composed of Cys149(403), Asp151(405), His205 (459) and Cys208(462). As for HICA, Arg153(407) is the detached partner of the Asp-Arg dyad characteristic of type I β-CAs. There is a functional equivalent of Gln151′ in PSCA, namely Gln394(140), but as for HICA, this (these) Gln residu(es) are not appropriately oriented to interact with alternate fourth coordination site ligands that might exchange with Asp151(405). Here again, the rotation of the loop containing two of the zinc ligands (151–155 or 405–409 for the two pseudo-monomers) compared to the functionally equivalent 162–166 loop in PSCA prevents the proper orientation of Gln394(140) close to Ser152(406). In PPCA, the Oγ of Ser152 is some 18 Å away from the Oε of Gln394. In addition, the distance from the main-chain amide Gly209 (463)–analogous to Gly224 in PSCA–is too far away (3.7 Å) from the zinc-bound oxygen of Asp151(405) to engage in a stabilizing hydrogen bond. The narrow, hydrophobic active site cleft is quite similar to other β-CAs. Prominent side chains in this cleft include Phe422(168), Ile173(427), Tyr444(190), and Tyr448(194).

3.4.2.3. Rv3588. In its monomeric crystal form, Rv3588 adopts a type II β-CA structure, with a pseudo-tetrahedral coordination shell composed entirely of protein ligands: Cys51, Asp53, His104 and Cys107. There is also a "broken" Asp53–Arg55 dyad, and Gln42′ and Ser54 do not interact to place Gln32′ in a position to coordinate to an alternate ligand bound to the zinc ion in place of Asp53. The typical, narrow hydrophobic channel, lined with Phe70′, Ala75, Tyr89′, and Val93′, leads to the active site zinc ion.

In the presence of thiocyanate ion, Rv3588 adopts an alternate, type I β-CA structure. The nitrogen atom of thiocyanate bonds to the zinc ion and displaces Asp53, which in turn interacts with Arg55 to form the Asp-Arg dyad that is characteristic of type I β-CAs. The formation of this dyad has rotated the 53–57 loop such that Ser54 has recruited Gln42′ to a position analogous to Gln151′ in PSCA. In this structure (PDB 2A5V) the side chain of Gln42′ has been interpreted to donate to, rather than receive a hydrogen bond from Ser54 [47]. Given the ambiguity in assigning the orientation of the amide group of Gln in X-ray crystallography, and the precedent provided by the eight other known β-CA structures in which this residue is poised to donate a hydrogen bond to a zinc-bound bicarbonate or bicarbonate analog, it seems plausible that the amide group of Gln42 in PDB 2A5V could be flipped 180° in order to meet that requirement. In this orientation, the distance between the amide nitrogen of Gln42′ and the nitrogen atom of thiocyanate is 4.8 Å, comparable to 4.1 Å for the Gln151′–zinc-bound oxygen distance in PSCA, or 4.4 Å for the His397-Nε2–water distance in HTCA. The real significance of the two Rv3588 structures is that they suggest that type II β-CAs are able to adopt two different conformations in solution, mediated by a reorientation of the active site Asp from acting as a zinc ligand to forming a dyad with the active site Arg residue. The alternate conformations of Rv3588 suggest a regulatory function for this behavior.

3.4.2.4. Summary of type II β-CA structure. Type II β-CAs are characterized by the following active site features: (1) a closed, four-coordinate $Cys_2HisAsp$ coordination sphere for zinc; (2) a broken Asp-Arg dyad; (3) the lack of a hydrogen bond donor (*e.g.*, Gln or His equivalent to Gln151′ in PSCA) in a position to interact with a bicarbonate ion bound in the position occupied by Asp, and (4) a narrow, hydrophobic active site cleft that lies along the dimer or pseudo-dimer interface, and leads to the active site zinc ion.

3.5. Some β-CAs possess a non-catalytic bicarbonate binding site

A non-catalytic bicarbonate binding site was discovered serendipitously in ECCA and HICA crystals soaked with bicarbonate [48]. Instead of binding to the active site zinc ion, bicarbonate ions were found to be bound to each monomer in a pocket about 8 Å away the zinc. The bicarbonate binding site is located near the dimerization interface and opposite the tetramerization interface (Fig. 4). A network of no less than 7 hydrogen bonds holds the bicarbonate ion in place. The indole nitrogen of Trp39, two of the guanidinium nitrogens of Arg64, the hydroxyl of Tyr181, and two water molecules all donate hydrogen bonds to the oxygen atoms of bicarbonate. One of these waters, denoted the "common" water, is found in the same location in many β-CAs, including PSCA, PPCA, Rv3588, ECCA, and HICA. This water accepts a hydrogen bond from the main-chain amide

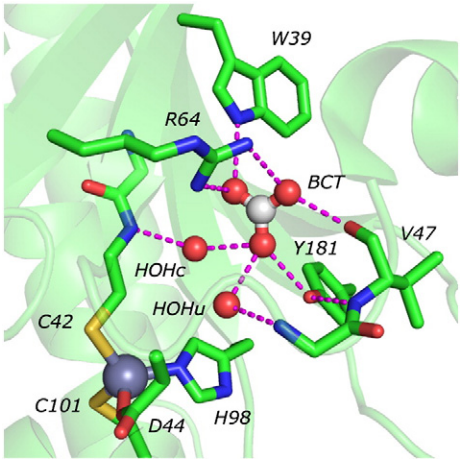

Fig. 4. Non-catalytic bicarbonate binding site of HICA (PDB 2A8D). Chain D is shown. BCT is bicarbonate; HOHc is the "common" water; HOHu is the "unique" water. Magenta dashes indicate hydrogen bonding interactions.

of Cys42. The other water, denoted the "unique" water, is found only in ECCA and HICA. This water molecule is positioned above the face of the imidazole ring of His98, where it can interact with the π-cloud, and accepts a hydrogen bond from the main-chain amide of Arg46. A seventh hydrogen bond exists between bicarbonate hydroxyl and the carbonyl oxygen of Val47. This is the lone hydrogen bonding interaction in which the bicarbonate ion is not a hydrogen bond acceptor. This arrangement of hydrogen bonds appears to be exquisitely designed to recognize bicarbonate ion: isoelectronic anions such as acetate or nitrate would be unable to fulfill all of the hydrogen bonding acceptor interactions from Trp39, Arg64, and Tyr181, while simultaneously donating a hydrogen bond to the main-chain carbonyl of Val47. The extensiveness of the hydrogen bonding network, requirement of low concentrations of bicarbonate ion (100 mM) to populate this site at full occupancy, the observation of the same interaction in two different β-CAs, and kinetics studies that reveal that bicarbonate ion is an inhibitor as well as a substrate for HICA (*vide infra*), suggest that this is not merely an adventitious anion binding site, but rather an integral functionality of the enzyme.

The binding of bicarbonate ion to the non-catalytic site enforces a type II β-CA structure: bicarbonate ion expels the side chain of Val47 from the binding site, which in turn reorganizes the Asp44–Pro48 loop, with two apparent consequences. First, the Asp44–Arg46 dyad is broken, allowing Asp44 to coordinate with the zinc ion, displacing the catalytically essential water molecule. Second, the rotation of Ser45 breaks the Ser45–Gln33′ interaction that orients Gln33′ to coordinate with zinc-bound bicarbonate. The Asp44–Pro48 loop orientation typical of type II β-CA is stabilized by bicarbonate, Tyr181, and the unique water molecule, which establish hydrogen bonds with the main-chain carbonyl of Val47, the amide nitrogen of Val47, and the amide nitrogen of Arg46, respectively.

The only β-CAs for which a non-catalytic binding site has been demonstrated are type II β-CAs, namely HICA and ECCA. However, all structurally characterized type II β-CAs have a Trp-Arg-Tyr bicarbonate binding triad, and this suggests the possibility that other type II β-CAs may harbor a non-catalytic bicarbonate binding pocket as well. Conspicuously, all structurally characterized type I β-CAs are missing one or more elements of the Trp-Tyr-Arg binding triad (Table 1). Thus an additional distinguishing characteristic between type I and type II β-CAs is the presence of a Trp-Arg-Tyr triad in the non-catalytic bicarbonate binding pocket.

4. Catalytic mechanism

The enzymes that have been most thoroughly kinetically characterized are SOCA, PSCA, ATCA, MTCA, and HICA. Steady-state kinetics parameters measured for these enzymes indicate that β-CAs, like all other CAs, are very fast enzymes, with k_{cat} values as high as $4\times10^5\,s^{-1}$ and k_{cat}/K_m values as high as $1.8\times10^8\,M^{-1}\,s^{-1}$ (Table 2). These values approach that of HCAII, among the fastest of known enzymes [56]. MTCA and HICA are significantly slower than the plant β-CAs. The catalytic mechanism of β-CA is believed to be parallel to that of α-CA (Fig. 5). This assessment is based on a number of observations. First, the structural organization the active site of β-CA maps rather well onto the active site of α-CA [43]. Second, β-CAs readily catalyze the isotopic exchange of O-18 in labeled HCO_3^- [30,57] in a way that can only be rationalized by the deposition of O-18 water on the active site zinc ion during catalysis. Third, there is a substantial body of kinetic evidence, summarized below, that *in toto* is difficult to accommodate by any other mechanism of action.

The basic mechanism for CO_2 hydration catalyzed by β-CA involves four steps. In the first step of the mechanism (1→2 in Fig. 5), CO_2 is concentrated in the active site by association with hydrophobic residues that line the active site cleft. (Recent crystallographic studies have shown that CO_2 binds to a similar hydrophobic pocket in HCAII [58].) CO_2 is then positioned for nucleophilic attack by zinc-bound hydroxide ion, the active species of the enzyme for CO_2 hydration. The hydroxide ion is oriented by the Asp residue of the Asp-Arg dyad so as to present its electron pairs to the incoming CO_2. In the second step of the mechanism (2→3 in Fig. 5), zinc-bound hydroxide undergoes a nucleophilic addition to CO_2, converting it to bicarbonate ion. The developing negative charge on the bicarbonate ion is stabilized by the donation of a hydrogen bond from a Gln residue (His in MTCA and HTCA). The zinc-bound bicarbonate ion can donate a hydrogen bond to the Asp residue of the Asp-Arg dyad. (In the reverse, bicarbonate dehydration reaction, this interaction would help the enzyme discriminate between HCO_3^- and other isoelectronic anions that cannot donate hydrogen bond to Asp.) In the third step of the mechanism (3→4 in Fig. 5) water exchanges for bicarbonate at the zinc ion, completing the CO_2-HCO_3^- interconversion steps. The final step of the CO_2 hydration mechanism (4→1 in Fig. 5) requires the loss of a hydrogen ion from zinc-bound water to regenerate the zinc-bound hydroxide ion. The ultimate acceptor of this hydrogen ion is exogenous buffer molecules, but there may be one or more intramolecular acceptors that could help transfer the proton away from the zinc-bound water, including the somewhat conserved Tyr residue in the hydrophobic pocket, and in PSCA and ATCA, a His residue near the exterior of the active site cleft.

Table 2
Steady-state kinetic parameters and solvent deuterium isotope effects for CO_2 hydration catalyzed by selected β-CAs.

	SOCA [30]	PSCA [59,60]	ATCA [57]	MTCA [52,65]	HICA [48]
k_{cat} (ms^{-1})	163 ± 1[a]	400[b]	320 ± 20[a]	24 ± 2 [c]	69 ± 29[a]
k_{cat}/K_m ($\mu M^{-1}s^{-1}$)	–	180[b]	68 ± 11[a]	8.3 ± 0.7 [c]	4.3 ± 0.8[a]
$\frac{k_{cat}^H}{k_{cat}^D}$	2.1 ± 0.2[d]	2.2[e]	–	2.1 ± 0.1[f]	–
$\frac{(k_{cat}/K_m)^H}{(k_{cat}/K_m)^D}$	1.2 ± 0.4[d]	0.6[e]	–	1.2 ± 0.1[f]	–

[a] Values of k_{cat} and k_{cat}/K_m represent maximal values at high pH.
[b] Values of k_{cat} and k_{cat}/K_m at pH 9.0.
[c] Values of k_{cat} and k_{cat}/K_m at pH 8.5.
[d] Determined at pH 9.0 in the presence of 40 mM buffer.
[e] Determined at pH 8.9 in the presence of 100 mM buffer.
[f] Determined at pH 8.5 in the presence of 50 mM buffer.

4.1. Rate-determining step

Multiple lines of evidence point to a rate-determining proton transfer step for β-CAs under most conditions. NMR measurements of the rate of CO_2-HCO_3^- exchange (all steps in Fig. 5 excluding the direct interconversion of 1 and 4) catalyzed by SOCA show that it is about 10× faster than the overall rate of catalysis [30]. For ATCA, O-18 isotope exchange experiments show that R_1, the rate of CO_2-HCO_3^- exchange at chemical equilibrium, is larger than R_{H_2O}, the rate of release of O-18 labeled water from the enzyme [57], a rate that is expected to require a proton transfer from an intra- or intermolecular donor to zinc-bound hydroxide during the conversion of HCO_3^- to CO_2. For SOCA [30], PSCA [59], and MTCA [52], there is a significant solvent deuterium isotope effect of about 2.0 on k_{cat} for the CO_2 hydration reaction, suggesting that the rate-determining step involves the transfer of one or more hydrogen ions; in addition, the solvent deuterium isotope effect on k_{cat}/K_m, which measures steps only from the binding of CO_2 to the release of HCO_3^-, is near unity. Therefore, the origin of the isotope effect must be localized to other steps in the mechanism than those involved in the interconversion of CO_2 and HCO_3^-, *i.e.*, the loss of a proton from zinc-bound water to regenerate zinc-bound hydroxide ion. Finally, k_{cat} for CO_2 hydration is found to be dependent on exogenous buffer concentration in a saturable way for SOCA [30], PSCA [59], MTCA [52], and ATCA [57]. As would be expected for the mechanism of Fig. 5, there is no buffer

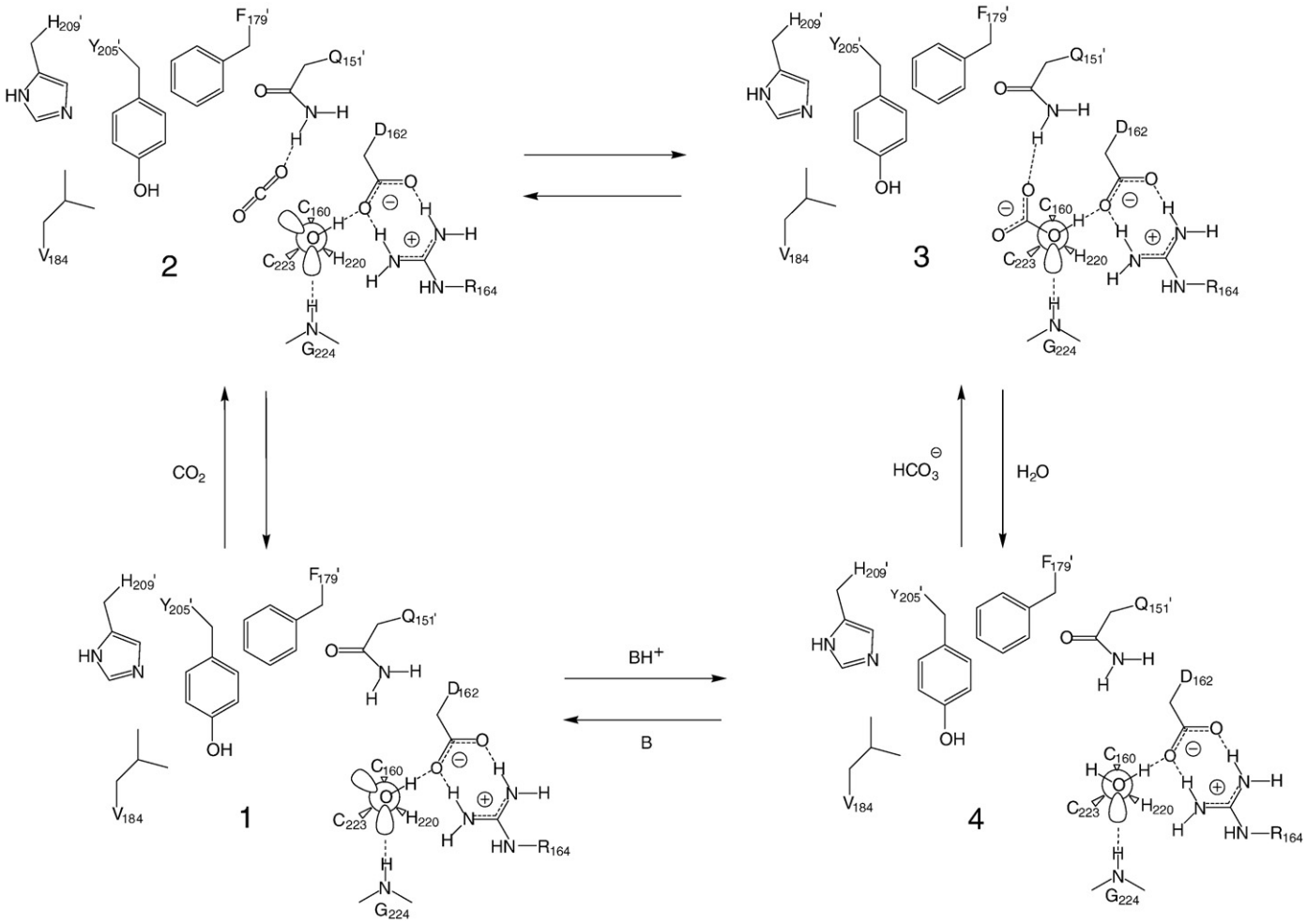

Fig. 5. Catalytic mechanism of β-CA. Residue numbering system is for PSCA; for other β-CAs see Table 1. The central sphere is the catalytically essential Zn^{2+} ion. "B" represents an exogenous hydrogen ion acceptor; "BH^{+}" represents an exogenous hydrogen ion donor. In MTCA and HTCA, a His residue substitutes for Gln151′ as a hydrogen bond donor to bicarbonate. CO_2 hydration reaction proceeds 1-2-3-4-1; HCO_3^- dehydration reaction proceeds 4-3-2-1-4. Figure adapted from [43].

concentration dependence for k_{cat}/K_m for CO_2 hydration, which relates only to CO_2-HCO_3^- exchange steps in this mechanism [59].

4.2. pH-rate profiles

For β-CA-catalyzed CO_2 hydration, both k_{cat} and k_{cat}/K_m increase with increasing pH [30,52,57,60]. This is consistent with the mechanism of Fig. 5. The pH profile of k_{cat} should reflect the efficiency with which endogenous or exogenous proton acceptors can accept a proton from the zinc-bound water species during catalysis. Therefore, one would expect k_{cat} to increase as the fraction of deprotonated proton acceptor species increases, and afford the pK_a value(s) of any intramolecular proton transfer species involved. The pH profile of k_{cat}/K_m should reflect the ionization state of the zinc-bound water molecule; again, one would expect k_{cat}/K_m to increase as the fraction of zinc-bound hydroxide increases, and the pH-rate profile should afford an estimate of the pK_a of the zinc-bound water molecule.

Unfortunately, the pH-rate profiles of β-CA-catalyzed CO_2 hydration are complex [52,60], likely involve more than one ionization in most cases, and are not easy to interpret. In addition, β-CAs frequently exhibit non-Michaelis–Menten kinetics [57,60]. For ATCA, the pH-rate profile for k_{cat}/K_m can be modeled by a titration curve of a single ionizable species with a pK_a of 7.2 ± 0.1 [30]. The H209A variant of PSCA also has a simple pH-rate profile for k_{cat}/K_m with an apparent pK_a value of 7.1 ± 0.1 [61]. These two results suggest that the zinc-bound water of plant β-CA has a pK_a near neutrality, and is similar to that of α-CAs, despite its considerably more electron-rich coordination environment. The pH-rate profile of k_{cat}/K_m for CO_2 hydration in HICA is highly cooperative, but it is possible to estimate a pK_a of 7.74 ± 0.04, significantly higher than for plant β-CAs. The pH-rate profiles for k_{cat} are complex for all β-CAs studied to date, but in ATCA, it is possible to identify two separate apparent pK_a values of 6.0 ± 0.8 and 8.8 ± 0.3 [57]. Thus, for plant CAs, it appears there may be at least two endogenous "proton shuttle" groups that assist the transfer of a proton from zinc-bound water during catalysis.

4.3. Site-directed mutagenesis studies of zinc-sphere residues

A number of site-directed β-CA variants have lent further support for the mechanism of Fig. 5. The ATCA variant Q158A has a significantly decreased maximal value of k_{cat}/K_m for CO_2 hydration at steady state, and a maximal value of $R_1/[E]$ that is an order of magnitude lower than that of the wild-type enzyme, while k_{cat} and $R_{H_2O}/[E]$ were largely unaffected [62]. This result strongly suggests that Gln158 in ATCA (equivalent to Gln151 in PSCA) is important for catalytic steps involving CO_2–HCO_3^- interconversion, and not proton transfer, a result consistent with its proposed role in Fig. 5.

A number of Asp-Arg dyad variants have also been studied. The replacement of Asp34 with Ala in MTCA reduces k_{cat} for CO_2 hydration by an order of magnitude in MOPS buffer, but not at all in imidazole buffer, suggesting that imidazole can rescue this variant. In addition, k_{cat}/K_m is relatively unaffected in this variant. This has led to the

suggestion that the dyad Asp may have an essential role in proton transfer. However, the replacement of the analogous Asp in SOCA [63] or HICA [64] results in nearly total loss of activity. Imidazole rescue of SOCA restores only 9% of the original activity at pH 8.0 [63]. These results suggest that the dyad Asp residue may have dual roles in the catalytic mechanism, in CO_2–HCO_3^- interconversion, and also in assisting proton transfer. The replacement of Arg36 in MTCA results in the reduction of k_{cat} and k_{cat}/K_m for CO_2 hydration by 2–3 orders of magnitude [65]. The variant can be partially rescued by exogenous guanidine, suggesting that the guanidinium group of Arg36 is the essential functionality required for catalysis [65]. This is as expected for the mechanism of Fig. 5: *i.e.*, Arg36 is required for the proper orientation of Asp34 to accept a hydrogen bond from zinc-bound hydroxide or bicarbonate.

4.4. Site-directed mutagenesis studies of proton transfer

In α- and γ-CAs there are readily identifiable intramolecular proton transfer groups (His64 in α-CA [56] and Glu84 in γ-CA[66]) that assist in the release of H^+ from zinc-bound water to buffers in bulk solution. Curiously, only the plant β-CAs have had site-directed mutagenesis studies performed specifically for the investigation of potential intramolecular proton transfer groups. Obvious candidates for intramolecular proton transfer groups in β-CA include the highly conserved active site tyrosine (Tyr205 in PSCA) and a histidine residue (His209 in PSCA) that lies at the mouth of the active site cleft in PSCA. In ATCA, the pH-rate profile of k_{cat} for CO_2 hydration suggests that there are two residues that can assist in proton transfer with pK_a values near 6.0 and 8.8. The variant H216N of ATCA has a pH-rate profile of k_{cat} whose low pH limb is greatly decreased compared to wild-type enzyme. Wild-type ATCA has a pH-rate profile of $R_{H_2O}/[E]$ with a characteristic double hump that suggests there are two possible, independent proton donor-acceptor pairs in the active site. One proton acceptor has an apparent pK_a of 7.7 ± 0.5, the other has a pK_a of ≈6.2. The lower pH "hump" of the pH-rate profile of $R_{H_2O}/[E]$ for ATCA is largely abolished in the H216N variant, suggesting that the pK_a of ≈6.2 belongs to His216 [57]. A qualitatively similar result is observed in the H209A variant in PSCA: the low pH region, but not the high pH region of the pH-rate profile of k_{cat} for CO_2 hydration is significantly decreased [61], but this result is not as clear as for ATCA. Additional evidence in support of His216 as an intramolecular proton transfer residue in ATCA is provided by chemical rescue of k_{cat} and R_{H_2O} in the H216N variant by exogenous histidine [57,67]. The higher pH "hump" of the pH-rate profile of $R_{H_2O}/[E]$ for ATCA is slightly but significantly diminished in the Y212F variant, suggesting that Tyr212 may have some role in proton transport in ATCA [57].

4.5. Inhibition of β-CA

Anions and sulfonamides, well-known inhibitors of α-CA, also inhibit β-CAs. The inhibition of plant β-CAs by anions and sulfonamides has been known for some time [30,60,68]. More recently, the inhibition of MTCA [69,70] and other β-CAs from *S. cerevisiae* [71,72], *H. pylori* [73], and *Candida albicans* and *Crytococcus neoformans* [74,75] has been investigated. Anions and sulfonamides presumably inhibit β-CA by the same mechanism as for α-CA, *i.e.* by binding to the zinc ion and displacing the catalytically essential water molecule. Support for this hypothesis is afforded by the X-ray crystal structure of the thiocyanate complex of Rv3588, in which the nitrogen atom of thiocyanate has displaced a water molecule from the fourth coordination site of the active site zinc ion [47]. A summary of inhibitor dissociation constants for selected anion and sulfonamide inhibitors of three β-CAs is shown in Table 3. In general, anions and sulfonamides are more potent inhibitors of plant β-CAs than archaeal (*e.g.*, MTCA), bacterial or yeast β-CAs. For inorganic monoanions, plant β-CAs have K_i values that are comparable to that of α-CAs, but for MTCA K_i values are typically 1–2 orders of magnitude larger. A similar trend is seen for sulfonamide inhibition. For α CAs, acetazolamide and ethoxzolamide have true K_i values in the nanomolar to sub-nanomolar range [76]. Although these sulfonamide inhibitors are among the most potent of β-CA inhibitors, they are several orders of magnitude weaker inhibitors of β-CAs than for α-CAs (Table 3). This is perhaps understandable, given the highly constricted nature of the β-CA active site. However, sulfamates, small sulfonamide-like molecules, are also relatively poor inhibitors of MTCA compared to α-CAs [69]. Interestingly, phenylboronic acid and phenylarsonic acid are moderately potent inhibitors of β-CAs, with K_i values in the high micromolar range [77]; these inhibitors are more potent inhibitors of β-CA than α-CA, and are a promising class of substances for β-CA-specific inhibition.

Table 3
Inhibition of selected β-CAs by some anions, sulfonamides and other compounds.

	K_i (mM)		
	SOCA[a] [30]	PSCA[b] [60]	MTCA[c] [69,77]
Cl^-	33	40	150
Br^-	–	–	42
I^-	–	0.18	13
CNO^-	–	0.020	11
SCN^-	0.075	–	0.52
N_3^-	0.0077	0.006	56
NO_3^-	0.20	0.035	7.8
SO_4^{2-}	43	190	950
Acetazolamide	–	0.028	0.012
Ethoxzolamide	–	0.0004	0.0054
Phenylboronic acid	–	–	0.20
Phenylarsonic acid	–	–	0.33

[a] pH 7.0, 25 °C.
[b] I_{50} values, pH 8.2–6.5, 2 °C.
[c] pH 7.4, 20 °C.

5. Allostery

Early investigations of the steady-state kinetics of type II β-CAs noted that these enzymes were inactive at neutral pH, and had rather unusual, steep pH-activity profiles [44,46]. Detailed kinetic studies of HICA-catalyzed CO_2 hydration at steady state and isotope exchange at chemical equilibrium clearly show highly cooperative behavior [48]. For example, at steady state k_{cat} is dependent on the loss of two H^+ for maximal activity, and k_{cat}/K_m has an apparent 4 H^+ dependence. In isotope exchange studies, the high pH limbs of both R_1 and R_{H_2O} require the cooperative gain of 2 H^+ for maximal HCO_3^- dehydration activity. Finally, the variation of both R_1 and R_{H_2O} with $[CO_2 + HCO_3^-]$ concentration is biphasic: at low $[CO_2 + HCO_3^-]$, both R_1 and R_{H_2O} increase with concentration in a Michaelis–Menten fashion; at higher concentrations, a highly cooperative inhibition is observed that apparently requires two molecules of inhibitor to cooperatively bind to inactivate the enzyme.

These kinetics results, in conjunction with the observation that bicarbonate ion binds to a non-catalytic site in HICA [48], strongly suggest that HICA is an allosteric enzyme that is regulated by HCO_3^-, and that the fundamental allosteric unit is a dimer. The working hypothesis is that the structures of the type II β-CAs represent the inactive, or T-state of the enzyme. The active, R-state, is presumably structurally similar to that of the type I β-CAs. The role of HCO_3^- is to stabilize the inactive, T-state of the enzyme through its interactions with Trp39, Arg64, Tyr181, and the main chain of the 44–48 loop. (The T-state of the enzyme is also apparently favored at low pH. The mostly likely explanation is that Asp44 can more easily displace zinc-bound water than zinc-bound hydroxide ion.) A schematic of the principal interactions involved in the T ⇆ R transition in HICA is summarized in Fig. 6. In the T-state, HCO_3^- displaces the side chain of Val47 and interacts with the allosteric triad of Trp39, Arg64, and Tyr181, as well as two water

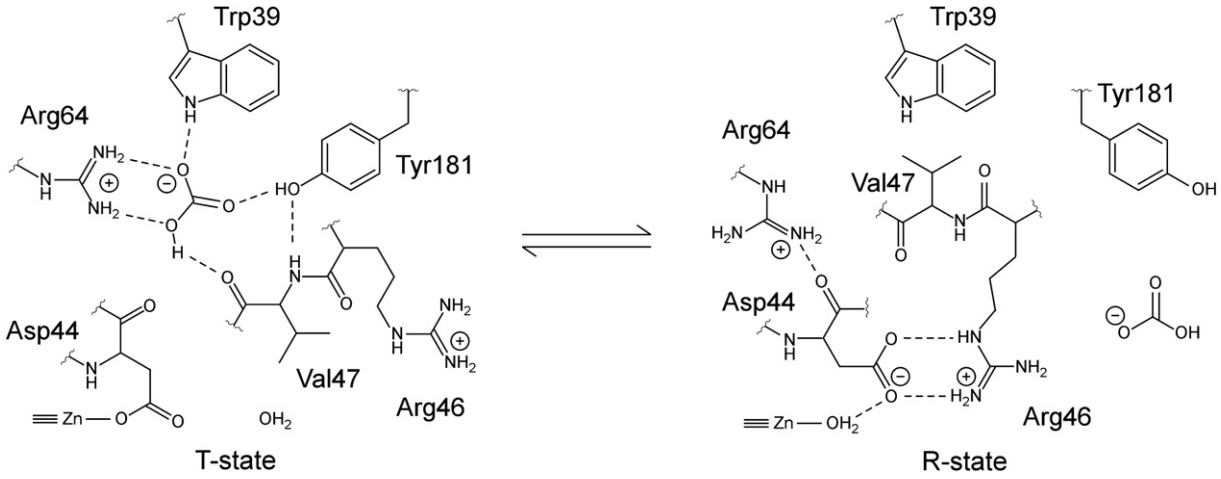

Fig. 6. Proposed mechanism of allosteric regulation of HICA by bicarbonate ion [48].

molecules (Fig. 4) and the main-chain carbonyl of Val47. This interaction displaces Arg46 from Asp44 and allows the latter residue to coordinate to the zinc ion, displacing the catalytically essential water molecule. In the absence of HCO_3^-, the side chain of Val47 can occupy the hydrophobic pocket provided by Trp39 and Tyr181, and the reorientation of the 44–48 loop allows Arg46 to reestablish contact with Asp44, allowing water to replace it as a zinc ligand. In addition, Arg64, released from its duties in binding to HCO_3^-, now helps to stabilize the R-state configuration of the 44–48 loop by establishing a hydrogen bond with the main-chain carbonyl of Asp44. Not shown in Fig. 6 is Ser45, which recruits Gln33′ to the active site and properly orients it for catalysis in the R-state conformation.

There is now significant evidence for alternate conformations of type II β-CAs. A "carboxylate shift" mechanism consistent with Fig. 6 has been directly observed in Rv3588, where the wild-type enzyme crystallizes in the T-state conformation, and the thiocyanate complex crystallizes in the R-state conformation [47]. However, HCO_3^- has not been observed to be complexed to Rv3588. Site-directed mutagenesis of HICA also supports allosteric regulation mechanism described by Fig. 6. While the HICA variant W39F still exhibits cooperativity, and exhibits substrate inhibition for R_1 and R_{H_2O}, the apparent K_i for HCO_3^- increases 4.8-fold in the variant enzyme [64]. This result is quantitatively consistent with the loss of a single stabilizing hydrogen bond in the allosteric binding site. The replacement of Tyr181 with Phe is less conclusive, and the resulting variant enzyme is about 1% as active as wild-type HICA. The HICA variant D44N, however, is particularly revealing. The replacement of Asp44 with Asn enforces the displacement of this residue from the zinc ion, and the crystal structure of HICA D44N clearly shows that a water molecule has coordinated to the zinc ion in place of the vacated amino acid side chain. In addition, the 44–48 loop of the enzyme has reorganized in a way that is astonishingly similar to the configuration of the corresponding residues in type I β-CAs. Indeed, the main-chain atoms of PSCA and HICA-D44N can be aligned to within 0.2 Å rms [64] (Fig. 7). This result strongly suggests that HICA is able adopt two alternate conformations: an active conformation resembling type I β-CA that has a catalytically essential zinc-bound water molecule, and an inactive conformation characteristic of type II β-CA, stabilized by bicarbonate ion, in which Asp44 displaces the zinc-bound water.

6. Outstanding questions

6.1. What is the extent and significance of allostery in β-CA?

While the binding of bicarbonate to an apparent allosteric regulation site has been demonstrated in only two β-CAs–HICA and ECCA–it seems likely that homologous proteins, including but not limited to PPCA, might also be allosterically regulated by bicarbonate ion. Indeed, Rv3588, which shares key sequence homology with HICA in the allosteric site region, exhibits highly cooperative pH dependence of activity [47]. Fig. 7 suggests several structural features that might distinguish between allosteric and non-allosteric β-CAs. The most obvious is the presence or absence of a complete Trp-Tyr-Arg triad that appears to be central to the recognition and stabilization of bicarbonate ion in the allosteric binding site. (PSCA has Val157 instead of the Trp39 of HICA.) More subtle differences between PSCA and HICA include the substitution of Ala159 (in PSCA) for Gly41 (in HICA), and a change in the sequence on the opposite side of the loop from Pro48–Ala49 (HICA) to Cys166–Pro167 (PSCA). The substitution of Ala for Gly in the allosteric binding site protrudes a methyl side chain into it that should provide significant steric interference to bicarbonate binding. In addition the "slippage" of the proline residue in the sequence of PSCA, relative to HICA, results in the proline ring protruding into, rather than away from the allosteric binding pocket. The net result is that the potential allosteric binding pocket of PSCA (and presumably related β-CAs) is exceedingly sterically crowded, and the confluence of Pro167, Val165, Ala159, and Val157 constitutes a hydrophobic cluster of side chains that might be difficult to disrupt.

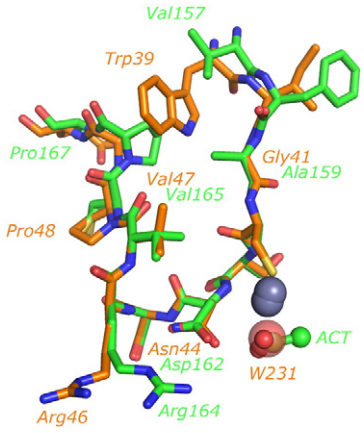

Fig. 7. Alignment of allosteric and active site residues of PSCA (PDB 1EKJ) and HICA-D44N (PDB 3E1V). Chain G of PSCA and chain A of HICA-D44N were used in the alignment. Carbon atoms of PSCA are colored green; HICA-D44N carbon atoms are colored orange. Zinc ions are depicted as gray spheres (HICA zinc ion is lower one). An acetate ion (ACT) bound to PSCA is depicted as a ball and stick model. Water-231, bound near the zinc ion in HICA-D44N, is depicted as a transparent sphere. Some key residues are labeled; green labels are for PSCA, orange labels are for HICA-D44N. From Ref. [64].

If this admittedly simplistic analysis is correct, it suggests that the evolutionary path from a non-allosteric to an allosteric β-CA (or *vice versa*) is not necessarily a complex one—it may require only 2–3 mutations to convert one to the other.

The physiological significance of β-CA allostery has not yet been demonstrated. Because bicarbonate ion is both an inhibitor and a product of the CO_2 hydration reaction catalyzed by β-CA, an allosteric β-CA essentially acts as a bicarbonate "thermostat." That is, allosteric β-CA is activated only when cellular bicarbonate concentrations are low. Complementation studies have not shed much light on this subject. ECCA is required for aerobic growth of *E. coli* under atmospheric CO_2 concentrations [38]. *E. coli* for which the ECCA gene has been deleted can be rescued in whole or in part by intracellular expression of *E. coli* CynT (a homolog of β-CA whose sequence in the allosteric site more closely resembles PSCA than HICA) or *Methanosarcina thermophila* γ-CA, the latter of which is certainly non-allosteric [38].

6.2. What is the ingress/egress route for allosteric bicarbonate?

An examination of the structures of HICA and ECCA reveals no obvious path for bicarbonate ion from the active site or from bulk solution to the allosteric pocket. How does bicarbonate ion enter the allosteric site? A possible clue is provided by the X-ray structure of the HICA variant Y181F. Crystals of this variant soaked in 100 mM bicarbonate ion clearly show a novel bicarbonate binding site in cleft of the dimerization interface on the exterior of the protein [64]. This bicarbonate ion is near, but not located in the allosteric site, and interacts with Arg64 and Glu50 residues from both protein chains in the fundamental dimer, and a water molecule. The rotation of the guanidinium group of either Arg64 residue would allow the migration of bicarbonate ion into the allosteric site.

6.3. Are there intramolecular proton transfer groups in non-plant β-CAs?

While site-directed mutagenesis has suggested that active site His and/or Tyr residues are important for proton transfer in ATCA [57] and PSCA [61], and that the active site Asp34 residue has a role in proton transport in MTCA [65], the role of the somewhat conserved Tyr residue (Tyr83 in HICA) as a proton shuttle group has not been examined by site-directed mutagenesis in a bacterial β-CA. For many non-plant β-CAs, this Tyr residue is the only likely intramolecular proton shuttle group. The equivalent of Tyr83 in HICA is missing in HTCA, MTCA and Rv1284. These proteins do not have any likely candidates for an intramolecular proton transfer group in the active site cleft. Perhaps this is why MTCA has a maximal k_{cat} value that is significantly smaller than that of HICA or plant β-CAs.

7. Conclusions

The β-CAs are perhaps the most diverse lot of the five currently known carbonic anhydrases, structurally and functionally. Although β-CAs exemplify the power of convergent evolution to "discover" the metal-hydroxide mechanism as the most efficient way to catalyze the interconversion of CO_2 and bicarbonate, they also have shown us something new: the first and only (to date) allosteric CA. Thus, the β-CAs not only have the potential to teach us about the optimization of enzyme catalysis, but also how molecular evolution goes about generating (or eliminating) allosterism. It seems likely that β-CA will continue to surprise, confound and illuminate.

Acknowledgements

The author wishes to acknowledge the support of the National Science Foundation (MCB-0741396 and CHE-0819686) for β-CA research at Colgate University.

References

[1] A.C. Neish, Chloroplasts. II. Their chemical composition and the distribution of certain metabolites between the chloroplasts and the remainder of the leaf, Biochem. J. 33 (1939) 300–308.
[2] K.S. Smith, J.G. Ferry, Prokaryotic carbonic anhydrases, FEMS Microbiol. Rev. 24 (2000) 335–366.
[3] K.S. Smith, C. Jakubzick, T.S. Whittam, J.G. Ferry, Carbonic anhydrase is an ancient enzyme widespread in prokaryotes, Proc. Natl. Acad. Sci. U. S. A. 96 (1999) 15184–15189.
[4] J.V. Moroney, S.G. Bartlett, G. Samuelsson, Carbonic anhydrases in plants and algae, Plant Cell Environ. 24 (2001) 141–153.
[5] S. Elleuche, S. Poggeler, Evolution of carbonic anhydrases in fungi, Curr. Genet. 55 (2009) 211–222.
[6] D. Hewett-Emmett, R.E. Tashian, Functional diversity, conservation, and convergence in the evolution of the α-, β-, and γ-carbonic anhydrase gene families, Mol. Phylogenet. Evol. 5 (1996) 50–77.
[7] J.N. Burnell, M.J. Gibbs, J.G. Mason, Spinach chloroplastic carbonic-anhydrase — nucleotide-sequence analysis of cDNA, Plant Physiol. 92 (1990) 37–40.
[8] N. Majeau, J.R. Coleman, Nucleotide sequence of a complementary DNA encoding tobacco chloroplastic carbonic anhydrase, Plant Physiol. 100 (1992) 1077–1078.
[9] C.A. Roeske, W.L. Ogren, Nucleotide sequence of pea cDNA-encoding chloroplast carbonic anhydrase, Nucleic Acids Res. 18 (1990) 3413-3413.
[10] C.A. Raines, P.R. Horsnell, C. Holder, J.C. Lloyd, *Arabidopsis thaliana* carbonic anhydrase: cDNA sequence and effect of carbon dioxide on mRNA levels, Plant Mol. Biol. 20 (1992) 1143–1148.
[11] J.P. Fett, J.R. Coleman, Characterization and expression of two cDNAs encoding carbonic anhydrase in *Arabidopsis thaliana*, Plant Physiol. 105 (1994) 707–713.
[12] J.V. Moroney, S.G. Bartlett, G. Samuelsson, Carbonic anhydrases in plants and algae, Plant Cell Environ. 24 (2001) 141–153.
[13] M.B. Guilloton, J.J. Korte, A.F. Lamblin, J.A. Fuchs, P.M. Anderson, Carbonic anhydrase in *Escherichia coli* — a product of the cyn operon, J. Biol. Chem. 267 (1992) 3731–3734.
[14] K.S. Smith, C. Jakubzick, T.S. Whittam, J.G. Ferry, Carbonic anhydrase is an ancient enzyme widespread in prokaryotes, Proc. Natl. Acad. Sci. U. S. A. 96 (1999) 15184–15189.
[15] K.S. Smith, J.G. Ferry, Prokaryotic carbonic anhydrases, FEMS Microbiol. Rev. 24 (2000) 335–366.
[16] K.S. Smith, J.G. Ferry, A plant-type (beta-class) carbonic anhydrase in the thermophilic methanoarchaeon *Methanobacterium thermoautotrophicum*, J. Bacteriol. 181 (1999) 6247–6253.
[17] G. Amoroso, L. Morell-Avrahov, D. Muller, K. Klug, D. Sultemeyer, The gene NCE103 (YNL036w) from *Saccharomyces cerevisiae* encodes a functional carbonic anhydrase and its transcription is regulated by the concentration of inorganic carbon in the medium, Mol. Microbiol. 56 (2005) 549–558.
[18] A.K.C. So, G.S. Espie, Cloning, characterization and expression of carbonic anhydrase from the cyanobacterium *Synechocystis* PCC6803, Plant Mol. Biol. 37 (1998) 205–215.
[19] M.R. Sawaya, G.C. Cannon, S. Heinhorst, S. Tanaka, E.B. Williams, T.O. Yeates, C.A. Kerfeld, The structure of beta-carbonic anhydrase from the carboxysomal shell reveals a distinct subclass with one active site for the price of two, J. Biol. Chem. 281 (2006) 7546–7555.
[20] M. Eriksson, J. Karlsson, Z. Ramazanov, P. Gardestrom, G. Samuelsson, Discovery of an algal mitochondrial carbonic anhydrase: molecular cloning and characterization of a low-CO2-induced polypeptide in *Chlamydomonas reinhardtii*, Proc. Natl. Acad. Sci. U. S. A. 93 (1996) 12031–12034.
[21] S. Mitsuhashi, T. Mizushima, E. Yamashita, M. Yamamoto, T. Kumasaka, H. Moriyama, T. Ueki, S. Miyachi, T. Tsukihara, X-ray structure of beta-carbonic anhydrase from the red alga, *Porphyridium purpureum*, reveals a novel catalytic site for CO2 hydration, J. Biol. Chem. 275 (2000) 5521–5526.
[22] R. Day, J. Franklin, Plant carbonic anhydrase, Science (Washington, DC, United States) 104 (1946) 363–365.
[23] A.J. Tobin, Carbonic anhydrase from parsley leaves, J. Biol. Chem. 245 (1970) 2656–2666.
[24] M. Kandel, A.G. Gornall, D.L. Cybulsky, S.I. Kandel, Carbonic anhydrase from spinach leaves. Isolation and some chemical properties, J. Biol. Chem. 253 (1978) 679–685.
[25] Y. Pocker, J.S.Y. Ng, Plant carbonic anhydrase. Properties and carbon dioxide hydration kinetics, Biochemistry 12 (1973) 5127–5134.
[26] S.R. MacAuley, S.A. Zimmerman, E.E. Apolinario, C. Evilia, Y.M. Hou, J.G. Ferry, K.R. Sowers, The archetype gamma-class carbonic anhydrase (Cam) contains iron when synthesized in vivo, Biochemistry 48 (2009) 817–819.
[27] Y. Xu, L. Feng, P.D. Jeffrey, Y.G. Shi, F.M.M. Morel, Structure and metal exchange in the cadmium carbonic anhydrase of marine diatoms, Nature 452 (2008) U53–U56.
[28] B.L. Vallee, D.S. Auld, Zinc coordination, function, and structure of zinc enzymes and other proteins, Biochemistry 29 (1990) 5647–5659.
[29] M.H. Bracey, J. Christiansen, P. Tovar, S.P. Cramer, S.G. Bartlett, Spinach carbonic-anhydrase - investigation of the zinc-binding ligands by site-directed mutagenesis, elemental analysis, and EXAFS, Biochemistry 33 (1994) 13126–13131.
[30] R.S. Rowlett, M.R. Chance, M.D. Wirt, D.E. Sidelinger, J.R. Royal, M. Woodroffe, Y.F. A. Wang, R.P. Saha, M.G. Lam, Kinetic and structural characterization of spinach carbonic anhydrase, Biochemistry 33 (1994) 13967–13976.
[31] V. Yachandra, L. Powers, T.G. Spiro, X-ray absorption spectra and the coordination number of zinc and cobalt carbonic anhydrase as a function of pH and inhibitor binding, J. Am. Chem. Soc. 105 (1983) 6596–6604.

[32] C. Kisker, H. Schindelin, B.E. Alber, J.G. Ferry, D.C. Rees, A left-handed beta -helix revealed by the crystal structure of a carbonic anhydrase from the archaeon *Methanosarcina thermophila*, EMBO J. 15 (1996) 2323–2330.
[33] E.H. Cox, G.L. McLendon, F.M.M. Morel, T.W. Lane, R.C. Prince, I.J. Pickering, G.N. George, The active site structure of Thalassiosira weissflogii carbonic anhydrase 1, Biochemistry 39 (2000) 12128–12130.
[34] M.B. Guilloton, A.F. Lamblin, E.I. Kozliak, M. Geraminejad, C. Tu, D. Silverman, P.M. Anderson, J.A. Fuchs, A physiological role for cyanate-induced carbonic anhydrase in *Escherichia coli*, J. Bacteriol. 175 (1993) 1443–1451.
[35] I. Nishimori, S. Onishi, H. Takeuchi, C.T. Supuran, The alpha and beta classes carbonic Anhydrases from *Helicobacter pylori* as novel drug targets, Curr. Pharm. Des. 14 (2008) 622–630.
[36] S. Mitsuhashi, J. Ohnishi, M. Hayashi, M. Ikeda, A gene homologous to beta-type carbonic anhydrase is essential for the growth of *Corynebacterium glutamicum* under atmospheric conditions, Appl. Microbiol. Biotechnol. 63 (2004) 592–601.
[37] H. Fukuzawa, E. Suzuki, Y. Komukai, S. Miyachi, A gene homologous to chloroplast carbonic anhydrase (icfA) is essential to photosynthetic carbon dioxide fixation by Synechococcus PCC7942, Proc. Natl. Acad. Sci. U. S. A. 89 (1992) 4437–4441.
[38] C. Merlin, M. Masters, S. McAteer, A. Coulson, Why is carbonic anhydrase essential to *Escherichia coli*? J. Bacteriol. 185 (2003) 6415–6424.
[39] R. Gotz, A. Gnann, F.K. Zimmermann, Deletion of the carbonic anhydrase-like gene NCE103 of the yeast *Saccharomyces cerevisiae* causes an oxygen-sensitive growth defect, Yeast 15 (1999) 855–864.
[40] D. Clark, R.S. Rowlett, J.R. Coleman, D.F. Klessig, Complementation of the yeast deletion mutant Delta NCE103 by members of the beta class of carbonic anhydrases is dependent on carbonic anhydrase activity rather than on antioxidant activity, Biochem. J. 379 (2004) 609–615.
[41] N. Majeau, M. Arnoldo, J.R. Coleman, Modification of carbonic anhydrase activity by antisense and over-expression constructs in transgenic tobacco, Plant Mol. Biol. 25 (1994) 377–385.
[42] N. Majeau, J.R. Coleman, Effect of CO2 concentration on carbonic anhydrase and ribulose-1, 5-bisphosphate carboxylase/oxygenase expression in pea, Plant Physiol. 112 (1996) 569–574.
[43] M.S. Kimber, E.F. Pai, The active site architecture of *Pisum sativum* beta-carbonic anhydrase is a mirror image of that of alpha-carbonic anhydrases, EMBO J. 19 (2000) 1407–1418.
[44] J.D. Cronk, J.A. Endrizzi, M.R. Cronk, J.W. O'Neill, K.Y.J. Zhang, Crystal structure of *E. coli* beta-carbonic anhydrase, an enzyme with an unusual pH-dependent activity, Protein Sci. 10 (2001) 911–922.
[45] P. Strop, K.S. Smith, T.M. Iverson, J.G. Ferry, D.C. Rees, Crystal structure of the "cab"-type beta class carbonic anhydrase from the archaeon *Methanobacterium thermoautotrophicum*, J. Biol. Chem. 276 (2001) 10299–10305.
[46] A.S. Covarrubias, A.M. Larsson, M. Hogbom, J. Lindberg, T. Bergfors, C. Bjorkelid, S.L. Mowbray, T. Unge, T.A. Jones, Structure and function of carbonic anhydrases from *Mycobacterium tuberculosis*, J. Biol. Chem. 280 (2005) 18782–18789.
[47] A.S. Covarrubias, T. Bergfors, T.A. Jones, M. Hoegbom, Structural mechanics of the pH-dependent activity of beta-carbonic anhydrase from *Mycobacterium tuberculosis*, J. Biol. Chem. 281 (2006) 4993–4999.
[48] J.D. Cronk, R.S. Rowlett, K.Y.J. Zhang, C.K. Tu, J.A. Endrizzi, J. Lee, P.C. Gareiss, J.R. Preiss, Identification of a novel noncatalytic bicarbonate binding site in eubacterial beta-carbonic anhydrase, Biochemistry 45 (2006) 4351–4361.
[49] S. Mitsuhashi, T. Mizushima, E. Yamashita, S. Miyachi, T. Tsukihara, Crystallization and preliminary X-ray diffraction studies of a beta-carbonic anhydrase from the red alga *Porphyridium purpureum*, Acta Crystallogr. D Biol. Crystallogr. Acta 56 (2000) 210–211.
[50] E. Krissinel, K. Henrick, Inference of macromolecular assemblies from crystalline state, J. Mol. Biol. 372 (2007) 774–797.
[51] A.K.C. So, G.S. Espie, E.B. Williams, J.M. Shively, S. Heinhorst, G.C. Cannon, A novel evolutionary lineage of carbonic anhydrase (epsilon class) is a component of the carboxysome shell, J. Bacteriol. 186 (2004) 623–630.
[52] K.S. Smith, N.J. Cosper, C. Stalhandske, R.A. Scott, J.G. Ferry, Structural and kinetic characterization of an archaeal beta-class carbonic anhydrase, J. Bacteriol. 182 (2000) 6605–6613.
[53] C.V. Hoang, H.G. Wessler, A. Local, R.B. Turley, R.C. Benjamin, K.D. Chapman, Identification and expression of cotton (Gossypium hirsutum L.) plastidial carbonic anhydrase, Plant Cell Physiol. 40 (1999) 1262–1270.
[54] I.M. Johansson, C. Forsman, Processing of the chloroplast transit peptide of pea carbonic anhydrase in chloroplasts and in *Escherichia coli*: identification of 2 cleavage sites, FEBS Lett. 314 (1992) 232–236.
[55] C. Forsman, M. Pilon, Chloroplast import and sequential maturation of pea carbonic-anhydrase — the roles of various parts of the transit peptide, FEBS Lett. 358 (1995) 39–42.
[56] D.N. Silverman, S. Lindskog, The catalytic mechanism of carbonic anhydrase: implications of a rate-limiting protolysis of water, Acc. Chem. Res. 21 (1988) 30–36.
[57] R.S. Rowlett, C. Tu, M.M. McKay, J.R. Preiss, R.J. Loomis, K.A. Hicks, R.J. Marchione, J.A. Strong, G.S. Donovan, J.E. Chamberlin, Kinetic characterization of wild-type and proton transfer-impaired variants of beta-carbonic anhydrase from *Arabidopsis thaliana*, Arch. Biochem. Biophys. 404 (2002) 197–209.
[58] J.F. Domsic, B.S. Avvaru, C.U. Kim, S.M. Gruner, M. Agbandje-McKenna, D.N. Silverman, R. McKenna, Entrapment of carbon dioxide in the active site of carbonic anhydrase II, J. Biol. Chem. 283 (2008) 30766–30771.
[59] I.M. Johansson, C. Forsman, Solvent hydrogen isotope effects and anion inhibition of CO2 hydration catalyzed by carbonic anhydrase from *Pisum sativum*, Eur. J. Biochem. 224 (1994) 901–907.
[60] I.M. Johansson, C. Forsman, Kinetic studies of pea carbonic anhydrase, Eur. J. Biochem. 218 (1993) 439–446.
[61] H. Bjorkbacka, I.M. Johansson, C. Forsman, Possible roles for His 208 in the active-site region of chloroplast carbonic anhydrase from *Pisum sativum*, Arch. Biochem. Biophys. 361 (1999) 17–24.
[62] R.S. Rowlett, C. Tu, P.S. Murray, J.E. Chamberlin, Examination of the role of Gln-158 in the mechanism of CO2 hydration catalyzed by beta-carbonic anhydrase from *Arabidopsis thaliana*, Arch. Biochem. Biophys. 425 (2004) 25–32.
[63] N.J. Provart, N. Majeau, J.R. Coleman, Characterization of pea chloroplastic carbonic anhydrase — expression in *Escherichia coli* and site-directed mutagenesis, Plant Mol. Biol. 22 (1993) 937–943.
[64] R.S. Rowlett, C. Tu, J. Lee, A.G. Herman, D.A. Chapnick, S.H. Shah, P.C. Gareiss, Allosteric site variants of *Haemophilus influenzae* β-carbonic anhydrase, Biochemistry 48 (2009) 6146–6156.
[65] K.S. Smith, C. Ingram-Smith, J.G. Ferry, Roles of the conserved aspartate and arginine in the catalytic mechanism of an archaeal beta-class carbonic anhydrase, J. Bacteriol. 184 (2002) 4240–4245.
[66] T.M. Iverson, B.E. Alber, C. Kisker, J.G. Ferry, D.C. Rees, A closer look at the active site of gamma-class carbonic anhydrases: high-resolution crystallographic studies of the carbonic anhydrase from *Methanosarcina thermophila*, Biochemistry 39 (2000) 9222–9231.
[67] C.K. Tu, R.S. Rowlett, B.C. Tripp, J.G. Ferry, D.N. Silverman, Chemical rescue of proton transfer in catalysis by carbonic anhydrases in the beta- and gamma-class, Biochemistry 41 (2002) 15429–15435.
[68] Y. Pocker, J.S.Y. Ng, Plant carbonic anhydrase. Hydrase activity and its reversible inhibition, Biochemistry 13 (1974) 5116–5120.
[69] S. Zimmerman, A. Innocenti, A. Casini, J.G. Ferry, A. Scozzafava, C.T. Supuran, Carbonic anhydrase inhibitors. Inhibition of the prokariotic beta and gamma-class enzymes from Archaea with sulfonamides, Bioorg. Med. Chem. Lett. 14 (2004) 6001–6006.
[70] S.A. Zimmerman, J.G. Ferry, C.T. Supuran, Inhibition of the archaeal beta-class (Cab) and gamma-class (Cam) carbonic anhydrases, Curr. Topics Med. Chem. 7 (2007) 901–908.
[71] S. Isik, F. Kockar, M. Aydin, O. Arslan, O.O. Guler, A. Innocenti, A. Scozzafava, C.T. Supuran, Carbonic anhydrase inhibitors: inhibition of the beta-class enzyme from the yeast *Saccharomyces cerevisiae* with sulfonamides and sulfamates, Bioorg. Med. Chem. 17 (2009) 1158–1163.
[72] S. Isik, F. Kockar, O. Arslan, O.O. Guler, A. Innocenti, C.T. Supuran, Carbonic anhydrase inhibitors. Inhibition of the beta-class enzyme from the yeast *Saccharomyces cerevisiae* with anions, Bioorg. Med. Chem. 18 (2008) 6327–6331.
[73] S. Morishita, I. Nishimori, T. Minakuchi, S. Onishi, H. Takeuchi, T. Sugiura, D. Vullo, A. Scozzafava, C.T. Supuran, Cloning, polymorphism, and inhibition of beta-carbonic anhydrase of *Helicobacter pylori*, J. Gastroenterol. 43 (2008) 849–857.
[74] A. Innocenti, F.A. Muhlschlegel, R.A. Hall, C. Steegborn, A. Scozzafava, C.T. Supuran, Carbonic anhydrase inhibitors: Inhibition of the beta-class enzymes from the fungal pathogens *Candida albicans* and *Cryptococcus neoformans* with simple anions, Bioorg. Med. Chem. 18 (2008) 5066–5070.
[75] A. Innocenti, R.A. Hall, C. Schlicker, F.A. Muhlschlegel, C.T. Supuran, Carbonic anhydrase inhibitors. Inhibition of the beta-class enzymes from the fungal pathogens *Candida albicans* and *Cryptococcus neoformans* with aliphatic and aromatic carboxylates, Bioorg. Med. Chem. 17 (2009) 2654–2657.
[76] S. Lindskog, Mechanism of sulfonamide inhibition of carbonic anhydrase, Chalmers Inst. Technol. Univ. Goteborg, Goteborg, Swed, 1969, pp. 157–165.
[77] A. Innocenti, S. Zimmerman, J.G. Ferry, A. Scozzafava, C.T. Supuran, Carbonic anhydrase inhibitors. Inhibition of the beta-class enzyme from the methanoarchaeon *Methanobacterium thermoautotrophicum* (Cab) with anions, Bioorg. Med. Chem. 14 (2004) 4563–4567.